Available online at www.sciencedirect.com
SCIENCE DIRECT
Journal of Power Sources 154 (2006) 171–179
JOURNAL OF POWER SOURCES
www.elsevier.com/locate/jpowsour

Current distribution mapping in polymer electrolyte fuel cells—A finite element analysis of measurement uncertainty imposed by lateral currents

R. Eckl [a,*], R. Grinzinger [a], W. Lehnert [b]

[a] *Institute for Energy Economy and Application Technology (IfE), Munich University of Technology, Arcisstr. 21, 80333 Munich, Germany*
[b] *Centre for Solar Energy and Hydrogen Research (ZSW), Helmholtzstr. 8, 89081 Ulm, Germany*

Received 9 February 2005; received in revised form 5 April 2005; accepted 9 April 2005
Available online 31 May 2005

Abstract

Using the finite element method, lateral currents in two different configurations for current distribution mapping in polymer electrolyte fuel cells (PEFCs) were simulated and the impact on the accuracy of measurement was analysed. The measurement techniques were of a conventional and a newly developed type, based on a segmented bipolar plate (BPP), respectively, a non-segmented bipolar plate combined with a printed circuit board (PCB). In both cases, neither the membrane electrode assemblies (MEAs) nor the gas diffusion layers (GDLs) were segmented and local currents were detected passively. The resistance of the measurement circuit and the current density gradient between neighbouring segments were found to be the major parameters causing current spreading. As expected, a significantly higher uncertainty of measurement could be observed and experimentally verified for the non-segmented bipolar plate. However, the accuracy is increasing with increasing homogeneity of the current density distribution. Achieving a uniform utilisation of the active area is a major task in fuel cell development and approaching this objective also improves the quality of measurement. Consequently, the application of non-segmented bipolar plates as highly flexible and practical measurement technique is a suitable option for current distribution mapping in technically relevant single cells and fuel cell stacks.

Keywords: Polymer electrolyte fuel cell; Current distribution; Lateral currents; Finite element modelling; Measurement uncertainty

1. Introduction

In order to achieve a better understanding of the electrochemical processes in polymer electrolyte fuel cells (PEFCs) and to investigate local effects of operating conditions and hardware configuration on cell performance, a variety of current distribution mapping techniques were developed and reported in the literature. Depending on the type of fuel cell to be analysed (laboratory scale single cells, cells of technical relevance and fuel cell stacks) and on the phenomena to be studied, the individual approaches differ with regard to methodology, spatial resolution and complexity.

By far, the majority of techniques used today are of an invasive nature, i.e. current distribution measurement is associated with constructional modifications of the PEFC hardware. Segmented bipolar plates (BPPs) in particular are primarily applied to laboratory scale single cells and consist of electrically insulated graphite or metal segments. Measurement of local currents is typically carried out outside the fuel cell either passively by ohmic resistors [1,2], Hall-effect sensors [3,4] or current transformers [5], or actively by multichannel-potentiostats [6,7]. Alternatively, a segmented BPP with integrated Hall-effect sensors for in situ current detection was documented by Wieser et al. [8].

For practical applications, BPPs are usually manufactured in a thin shape for volume, weight and cost reduction. Consequently, any segmentation is difficult to achieve if mechanical strength must be guaranteed at the same time. Assuming that the ratio between through-plane and in-plane conductivity of thin BPPs is high, however, lateral currents can be neglected and segmentation can be omitted [9,10]. Following this as-

* Corresponding author. Tel.: +49 89 289 23977; fax: +49 89 289 28313.
E-mail address: reckl@ewk.ei.tum.de (R. Eckl).

0378-7753/$ – see front matter © 2005 Elsevier B.V. All rights reserved.
doi:10.1016/j.jpowsour.2005.04.004

Nomenclature

$\vec{E}$	vector of electric field strength ($V\,m^{-1}$)
i	relative segment current (%)
I	electric current (A)
$\vec{j}$	vector of electric current density ($A\,m^{-2}$)
R	electric resistance (Ω)
u	uncertainty (%)

Greek letters

δ	boundary layer thickness (m)
φ	scalar electric potential (V)
σ	electric conductivity (scalar/tensor) ($S\,m^{-1}$)

Subscripts

0	boundary condition
BPP	bipolar plate
c	contact
eff	effective tensor component
GDL	gas diffusion layer
M	measurement circuit
meas	measurement
mod	modelling/simulation
n	segment index (11. . .33)
S	shunt
x, y, z	x-, y-, z-direction

sumption, an approach with "quasi-segmented" BPPs was developed and applied to single cell direct methanol fuel cells by Geiger [9], consisting of a thin non-segmented BPP, metallic current collectors on the backside and external sensors. The gap, respectively, the uncovered area between neighbouring current collectors additionally suppresses lateral currents. An alternative approach labelled the semi-segmented plate principle makes use of a segmented graphite plate attached to a thin, non-segmented BPP. Local currents are either measured externally as with the "quasi-segmented" cell [10] or the ohmic voltage drop across the individual segments is detected in situ and the respective currents are calculated [11].

A further invasive method for current distribution mapping is the replacement of a BPP by a printed circuit board (PCB) containing gas channels and current collectors on the ribs between channels. In the case of a simple PCB, local currents are conducted to the backside by plated through-holes and fed to a sensing device, e.g. a multichannel-potentiostat [12,13]. If the PCB is manufactured in a multilayer design, current sensors such as shunt resistors [14] or a combination of coils [15] can be integrated into the board and connected by circuit paths in the intermediate layers. Obviously, this configuration is particularly capable for current distribution measurements in fuel cell stacks because a compact design and flexible arrangement of the wiring is possible.

A non-invasive method for the measurement of current density distributions in fuel cells is given by magnetotomography. The approach is based on the fact that an electric current flowing in a conductor, e.g. a piece of wire, generates a circular magnetic field. Applied to fuel cells, sensors detect the magnetic field around a single cell or a stack and the underlying current density distribution is calculated with the aid of numerical techniques. Thus, current density measurement without any drawbacks on fuel cell operating conditions is possible. However, magnetotomography is as yet in an early development stage and only allows for relative measurements in steady state [16].

A major problem associated with invasive measurement techniques is the occurrence of lateral currents, most notably if non-segmented components are used. As a consequence, a blurring of the current density sets in, causing an increased measurement uncertainty. In other words, current spreading in non-segmented BPPs and gas diffusion layers (GDLs) causes the measured current density distribution to be more homogeneous than it appears at the electrode. Within the scope of this paper, two different approaches for current distribution mapping are chosen and the respective cell configurations are modelled. With the aid of the finite element method, lateral currents are calculated and drawbacks on the accuracy of measurement are analysed.

2. Scope of finite element modelling

For most of the invasive current distribution mapping techniques mentioned above, it is assumed that the ratio between through-plane and in-plane conductivity of the electrode and GDL is high due to the small layer thickness. Thus, the flow direction of the electric current generated at the triple phase boundary will primarily be perpendicular to the plane of the membrane electrode assembly (MEA) and a segmentation of the electrode and GDL as proposed in several studies, e.g. [7,11,17], is not necessary. On one hand, avoiding segmentation at the place of electrochemical current generation is desirable to preserve true fuel cell operation characteristics and avoid highly individualized specialty MEAs [6]. On the other hand, however, for a correct interpretation of measured current density distributions, it must be resolved to what extent the assumption of negligible current spreading is valid, respectively, what measurement uncertainty must be tolerated.

Based on experimental and model results, Natarajan and Van Nguyen [17] recommend a segmentation of both anodic and cathodic current collectors, respectively, BPPs as well as the MEA and GDL to suppress lateral currents and to eliminate effects of contact resistance variations on current density distribution. However, the fuel cell configuration used by the authors is highly specific and only one single channel is regarded. In the case of a real two-dimensional measurement with high resolution, a significant proportion of the active area may be electrochemically inert through the insertion of insulation layers into the MEA. Alternatively, potentiostatic operation of individual segments helps to sup-

press lateral currents by partially avoiding a gradient of the electric field strength between neighbouring segments. For high spatial resolution or simultaneous current distribution measurements at several single cells in a fuel cell stack, however, the implementation effort is rather high and expensive due to the multichannel-potentiostat required for this approach. Thus, the focus of this study is concentrated on non-segmented MEAs and GDLs and on passive current detection techniques.

Despite of an inherently low measurement resistance associated with the magnetic loop current detection system described by Wieser et al. [8], a maximum measurement error of 5% was reported. Noponen et al. [18] used a segmented bipolar plate and 100 mΩ precision resistors for current distribution measurements, resulting in a maximum uncertainty around 10%. From these examples with segmented BPPs and non-segmented MEAs/GDLs documented in the literature, it can be concluded that the occurrence of lateral currents is strongly dependent on the geometric configuration, material parameters and the resistance of the measurement circuit. Furthermore, it is obvious from these observations that significant lateral currents can be expected in the case of non-segmented BPPs. The thickness of practical BPPs varies in the range of 0.1 mm for corrugated stainless steel sheeting up to several millimetres for graphite composite plates. Considering not only the geometric but also the electrical properties, especially graphite BPPs tend to have higher intrinsic conductivities in in-plane direction than through-plane. Therefore, depending on the ratio between through-plane and in-plane conductivity and on the geometric parameters, more or less pronounced current spreading will set in. Even though non-segmented, respectively, semi-segmented BPPs are already used for current distribution measurement in practice, only rough estimates concerning lateral currents and the resulting measurement uncertainties have been published for these methodologies [9].

For a quantitative analysis of lateral currents in different hardware configurations, two techniques have been modelled in this study. The first one depicted in Fig. 1a is representative for state of the art technologies comprising a segmented BPP at the anode side of a single cell with individual current collectors and external sensors. The current sensors are modelled as ohmic resistors R_M and neither the electrodes nor the GDL are segmented. The second configuration depicted in Fig. 1b represents a new development on the basis of preceding approaches for current distribution mapping, respectively, the PCB technology and the semi-segmented plate principle. The measurement system comprises a non-segmented BPP in combination with a PCB at the anode side of a PEFC. Again, electrodes and GDLs are not segmented. Local currents are measured by means of shunt resistors R_S integrated into the PCB using a multilayer design. With regard to stack integration, the PCB contains channels for a coolant. The individual current collectors are placed on the lands between cooling channels and are plated with gold in order to avoid corrosion

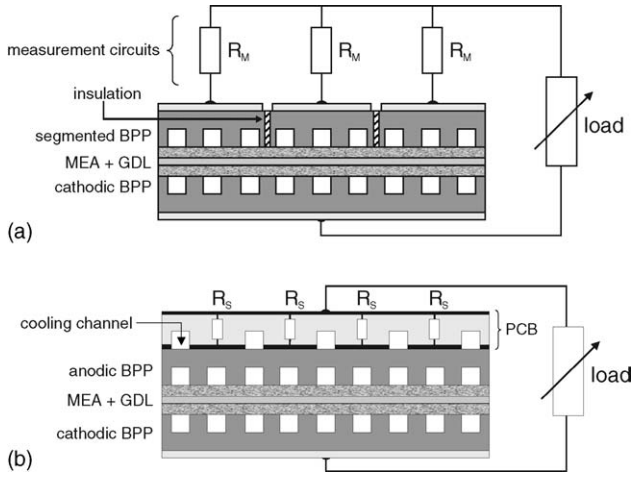

Fig. 1. Schematic of cell configurations for finite element modelling: (a) segmented bipolar plate and (b) non-segmented bipolar plate and printed circuit board at the anode side of a single cell (MEA, membrane electrode assembly; GDL, gas diffusion layer; BPP, bipolar plate; PCB, printed circuit board; R_M, measurement circuit resistor and R_S, shunt resistor).

and minimize contact resistance. Depending on the desired spatial resolution, several current collectors can be grouped together and assigned to one single shunt resistor. Electrical connections between current collectors, sensor resistors and a conductive layer on the backside of the PCB are provided by plated through-holes. The main advantages of this newly developed method can be summarized as follows: (i) the PCB can be manufactured in a shape that guarantees for compatibility with the anodic bipolar plate in a single cell, respectively, with adjacent bipolar plates in a fuel cell stack; (ii) the sense wires associated with the individual resistors can be integrated into the PCB and connected to a data acquisition unit from the edge of the PCB; (iii) thus, stack integration at any position is possible; (iv) high flexibility due to modular configuration, i.e. different BPPs can be tested with a single PCB as long as certain design parameters (e.g. internal manifolding) remain unchanged and (v) as with a semi-segmented plate, the fluid dynamic properties for the reactant gases as well as the electrical and thermal conductivities of the PEFC are conserved to the greatest possible extent.

Basis for the simulations was a PEFC layout provided by the Centre for Solar Energy and Hydrogen Research in Ulm/Germany with 100 cm^2 active area. Anode side BPPs are 1.5 mm thick with a serpentine type flowfield as shown in Fig. 2a. The channel width is 1.0 mm, channel depth 0.3 mm and the width of the landings between channels is 1.0 mm. In Fig. 2b, the parallel channel cooling flowfield integrated into the PCB is depicted. Cooling channels are 1.5 mm wide and 0.6 mm deep; the width of landings is 3.0 mm. It can also be seen from Fig. 2b that a spatial resolution of 3×3 segments was assumed, i.e. seven, respectively, eight current collectors are grouped together and connected to a single

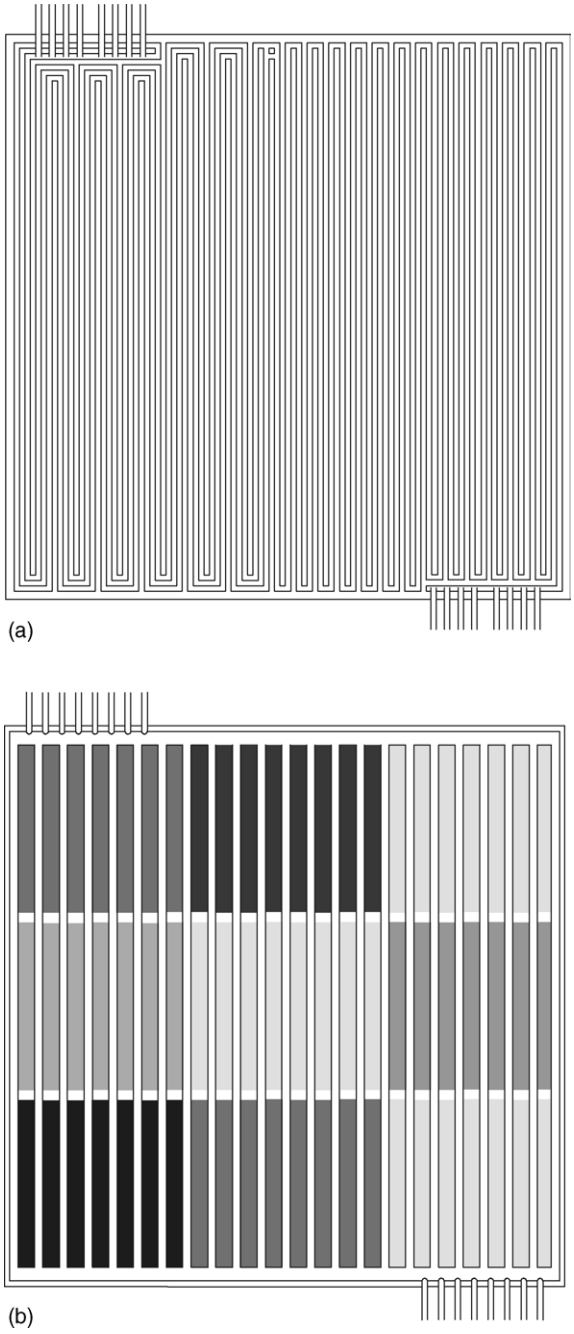

Fig. 2. (a) Anode side gas flowfield and (b) cooling flowfield of printed circuit board with current collectors configured in a 3×3 segment pattern.

shunt resistor.[1] In an analogous manner, the segmented BPP was assumed to be divided into 3×3 segments by insulation layers (e.g. an epoxy resin material) of 0.5 mm thickness.

[1] It should be noted that the term segment is used in this study both for segmented as well as for non-segmented BPPs. In the case of a non-segmented BPP, the area beneath one or more current collectors associated with one single current sensor is considered a segment.

3. Model equations, methodology and material parameters

The current generated by PEFC is DC and modelling was carried out in three dimensions for stationary states in conductive media. Problems of this type are described by Laplace's equation

$$\nabla(\sigma\nabla\varphi) = 0, \tag{1}$$

respectively,

$$\frac{\partial}{\partial x}\left(\sigma_x\frac{\partial\varphi}{\partial x}\right) + \frac{\partial}{\partial y}\left(\sigma_y\frac{\partial\varphi}{\partial y}\right) + \frac{\partial}{\partial z}\left(\sigma_z\frac{\partial\varphi}{\partial z}\right) = 0, \tag{2}$$

where φ represents the scalar electric potential and σ_x, σ_y, and σ_z are the components of the electric conductivity tensor σ. Furthermore, Ohm's law describes the correlation between current density $\vec{j}$ and the electric field strength $\vec{E}$:

$$\vec{j} = \sigma \times \vec{E}. \tag{3}$$

The correlation between electric field $\vec{E}$ and electric potential φ is:

$$\vec{E} = -\nabla\varphi. \tag{4}$$

Thus, follows from Eqs. (3) and (4):

$$\vec{j} = -\sigma \times \nabla\varphi, \tag{5}$$

i.e. the simulation of electric currents requires the solution of Laplace's equation. For this purpose, the FEMLAB® software package with integrated geometric modelling and post-processing capabilities was used in this study.

As the cathode side remains unchanged for the two measurement techniques, the simulation can be restricted to the anode side alone. The objective was a quantification of lateral currents in the components GDL and BPP and no electrochemical processes were simulated. Current generation at the electrode was modelled by a Neumann type boundary condition with a defined normal component of the inward current density. Furthermore, a uniform compression of the GDL was assumed, i.e. no distinction was made between areas beneath channels and ribs of the BPP. From this follows a constant thickness and a constant through-plane conductivity of the GDL across the entire active area. The ohmic resistances of the individual measurement circuits were incorporated into the simulation by applying Dirichlet type boundary conditions at the current collector locations, i.e. by defining equipotential surfaces. The individual voltage values were calculated by integrating the current density beneath the respective current collectors and multiplication of the resulting segment current by the ohmic resistance of the measurement circuit. As the numerical solution of differential equations is carried out iteratively in FEMLAB®, currents and potentials are recalculated within each iteration step until convergence is reached.

The contact resistance between GDL and BPP was modelled by thin film approximation [19]. Assuming a

negligible tangential component of the current density vector and a constant conductivity σ_c in the boundary layer, a one-dimensional approximation in normal direction (z-direction) can be derived from Eq. (2):

$$-\sigma_c \frac{\partial^2 \varphi}{\partial z^2} = 0. \tag{6}$$

This equation can be solved analytically by applying the potentials φ_{BPP} and φ_{GDL} to the upper and lower edges of the boundary layer with thickness δ:

$$\varphi(z) = \frac{\varphi_{BPP} - \varphi_{GDL}}{\delta} z + \varphi_{GDL}. \tag{7}$$

Together with Eq. (5), this yields:

$$j_z = -\sigma_c \frac{\varphi_{BPP} - \varphi_{GDL}}{\delta}. \tag{8}$$

For the simulation, the GDL and BPP were implemented in two separate submodels with variables φ_{GDL} and φ_{BPP}. Eq. (8) connects the submodels by defining a Neumann type boundary condition in each case. As current outflow from the GDL represents current inflow into the BPP, the boundary conditions have opposite sign in the respective submodels. With regard to the surface between BPP and current collectors, gold plated metal sheets with a negligible contribution to contact resistance were assumed in the simulation and Dirichlet type boundary conditions as described above were directly applied to the BPP surface.

Due to the fact that each segment is surrounded by at least three neighbouring segments, a detailed analysis of lateral currents requires three-dimensional modelling. For the complex flowfield structure of the BPP, this results in considerable computing time and quickly imposes memory problems when a standard PC is used. Furthermore, the individual components feature strongly unequal volume and surface dimensions that have to be addressed by the discretisation scheme. An approach to solve these problems is the numerical volume averaging method (NVAM), i.e. replacing details of the original structure by their averaged counterparts as described by Roos et al. [20]. For this purpose, "virtual experiments" on a repetitive region are carried out and tensor components for a representative volume element are "measured" using the finite element method.

In Fig. 3, repetitive and representative volume elements for the given anode side bipolar plate are depicted. The repetitive structure comprises a channel unit and half a rib at each side. This element was modelled and the electric conductivities of the BPP material adopted. As in practical experiments, differential voltages were applied consecutively in x-, y- and z-direction by defining Dirichlet type boundary conditions at opposite surfaces. At the remaining surfaces, homogeneous Neumann conditions with zero normal current density were applied. The current flowing through the element was evaluated numerically in each direction and finally the effective conductivities were calculated by taking into account the geometric properties of the representative volume element. Thus, the complex geometry of the BPP with integrated gas channels was transformed into a simple structure that could be simulated with a standard desktop computer. Through the volume averaging process, all the information about the underlying BPP structure was cast into the anisotropy of the effective conductivity parameters.

In the PEFC generation used for this study, BPPs are manufactured from the graphite-PVDF-compound SIGRACET® BMA 5 with specific electrical conductivities of 100 S cm^{-1} in-plane and 20 S cm^{-1} through-plane. NVAM yields for the effective conductivities of the BPP $\sigma_{x,\text{eff}} = 90$ S cm^{-1}, $\sigma_{y,\text{eff}} = 83$ S cm^{-1} and $\sigma_{z,\text{eff}} = 16$ S cm^{-1}. Compared to the conductivity in y-direction, the higher conductivity in x-direction is due to the alignment of the ribs. As GDL material, SIGRACET® GDL 10 BB carbon paper was assumed with specific electrical in-plane resistances of 0.7 Ω square^{-1} in machine direction and 1.2 Ω square^{-1} in cross machine direction. Through-plane, both the resistance as well as the thickness of the GDL are strongly dependent on the mechanical pressure. For the simulation, a surface pressure of 17 bar was assumed, which is equivalent to a compression of the GDL to 75% of its original thickness and corresponds to the conditions in a fuel cell stack. From this follows a thickness of 0.32 mm and a specific electrical through-plane resistance of 9.1 mΩ cm^2.

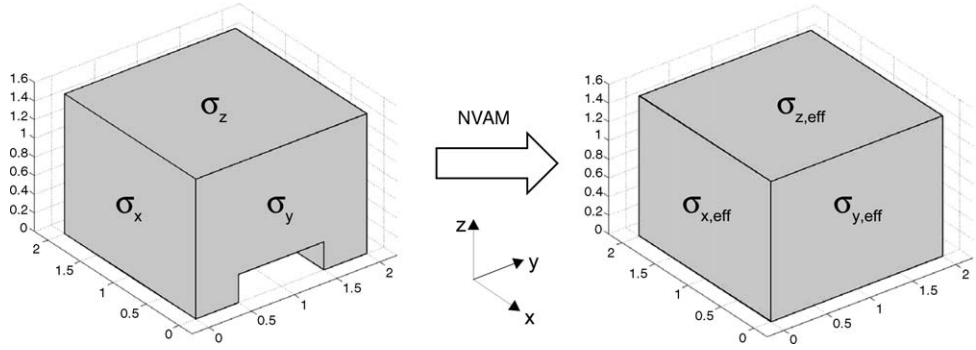

Fig. 3. Repetitive geometric structure (left) and representative volume element with anisotropic material behaviour (right) for the anode side bipolar plate (NVAM, numerical volume averaging method).

Table 1
Electrical conductivities for finite element modelling of lateral currents (bipolar plate material SIGRACET® BMA 5, gas diffusion layer SIGRACET® GDL 10 BB, mechanical pressure 17 bar)

Bipolar plate (S cm^{-1})	
In-plane	100
Through-plane	20
Numerical volume averaging (S cm^{-1})	
x-Direction, effective	90
y-Direction, effective	83
z-Direction, effective	16
Gas diffusion layer (17 bar) (S cm^{-1})	
In-plane, machine direction	45
In-plane, cross machine direction	26
Through-plane	3.5
Boundary layer, contact resistance (17 bar) (S cm^{-1})	200

Concerning the contact resistance between GDL and BPP, no values were available for the combination of SIGRACET® GDL 10 BB and SIGRACET® BMA 5. For this reason, measured data for graphite and carbon-fiber paper (Toray, 3.5 wt% Teflon) as documented by Mathias et al. [21] were applied. At a surface pressure of 17 bar, a contact resistance of 5.0 mΩ cm^2 is given. This corresponds to a specific electrical conductivity of 200 S cm^{-2}, which represents the numerical value of σ_c/δ in Eq. (8). In Table 1, the electrical material parameters for the individual layers used in the simulation are summarized with consistent units. BPP and GDL material data were obtained from the manufacturer SGL Technologies (Meitingen/Germany).

4. Simulation results for the segmented bipolar plate and external sensors

For the purpose of a worst-case estimation, a strongly inhomogeneous current distribution with constant current density beneath the central segment and zero current density beneath the surrounding segments was assumed. In Fig. 4, the simulation results expressed as relative segment currents i_n are depicted against the measurement circuit resistance R_M. Relative segment currents are derived from the integral segment currents I_n through the equation $i_n = I_n/I_0 \times 100\%$, with n representing the segment index and I_0 representing the total current flowing into the structure, i.e. the electrochemically generated current beneath the central segment modelled by a Neumann type boundary condition with constant current density in normal direction.

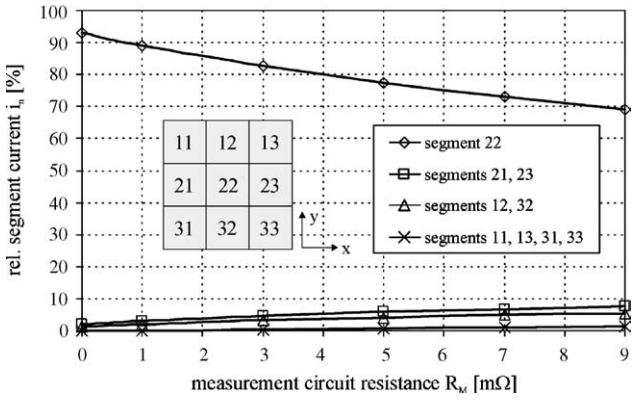

Fig. 4. Relative segment currents i_n against measurement circuit resistance R_M and position of segments across the active area (segmented bipolar plate, 3 × 3 segments).

The measurement circuit resistance R_M was varied between 0 and 9 mΩ, a range that reflects many state of the art measurement techniques. It can be noted from Fig. 4 that the relative segment current across the central segment 22 decreases with increasing R_M and that relative currents across the surrounding segments increase. $R_M = 0$ can be interpreted as galvanostatic operation mode with all the individual segment voltages forced to be constant by a multichannel-potentiostat. In this case, about 7% of I_0 are flowing in lateral direction within the GDL, i.e. the measured current density distribution is always more homogeneous than the distribution occurring at the electrode because of the inherent through-plane resistances of the GDL and of the graphite segments. Segments 12, 21, 23 and 32, which are conterminous with the central segment, show the highest proportion of lateral currents. In contrast, lateral currents across the corner segments 11, 13, 31 and 33 are almost negligible. Furthermore, it can be noted that currents occurring at segments 21 and 23 are higher than those occurring at segments 12 and 32. This is due to the fact that the machine direction of the GDL with higher electric conductivity was applied in x-direction of the model geometry.

The strongly inhomogeneous current density distribution with current generation only beneath the central segment represents a rather theoretical assumption. Steep gradients cannot be excluded, but at least a continuous current density characteristic can be expected in reality. Another extreme example is defined by a perfectly homogeneous distribution across the active area. Simulations with R_M between 0 and 9 mΩ revealed no significant lateral currents for this operating state. Thus, it can be concluded that current spreading is strongly dependent on the magnitude of R_M and on the current gradient between neighbouring segments, respectively, the gradient within a domain on both sides of the insulation layer. The simulated current density distributions—strongly inhomogeneous and perfectly homogeneous—mark the upper and lower boundaries for the measurement uncertainty caused by lateral currents in the GDL at constant R_M. With increasing current density gradient and consequently with increasing voltage difference between neighbouring current collector surfaces, the measurement error is also increasing.

5. Simulation results for the non-segmented bipolar plate and printed circuit board

In analogy to the previous chapter, a strongly inhomogeneous current density distribution with current generation

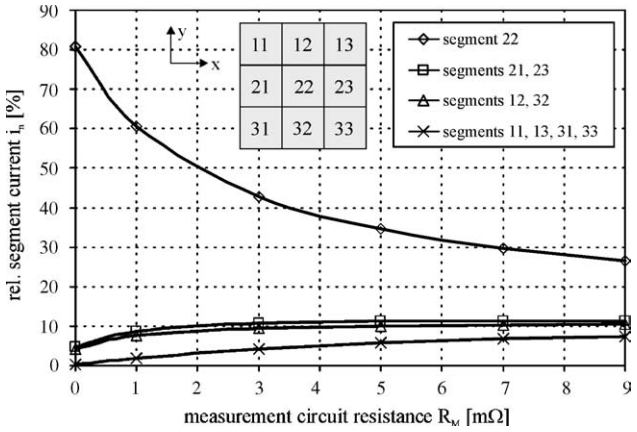

Fig. 5. Relative segment currents i_n against measurement circuit resistance R_M and position of segments across the active area (non-segmented bipolar plate and printed circuit board, 3 × 3 current sensors).

only beneath the central segment was modelled for a first approach and the simulation results are expressed as relative segment currents in Fig. 5. It should be noted that PCB measurement circuit resistances include the individual shunt resistors R_S for current sensing, plated through-holes and internal wiring. Due to the in-plane conductivity between neighbouring segments both in the GDL as well as in the non-segmented BPP, significantly higher lateral currents can be observed. The highest proportion occurs across segments 12, 21, 23 and 32 again. However, in contrast to the segmented BPP, lateral currents across the corner segments 11, 13, 31 and 33 cannot be neglected any more because of the unhindered cross-flow of electric current in the BPP. Compared to segments 12 and 32, the higher currents across segments 21 and 23 can be attributed to the orientation of the GDL machine direction and BPP channel direction along the *x*-axis of the model geometry.

In order to test the methodology with non-segmented BPP and PCB in practice, a prototype PCB with 3 × 3 segments, cooling flowfield according to Fig. 2b and measurement circuit resistances of 7 mΩ (±0.1 mΩ) was manufactured. With the aid of this prototype PCB, the simulation results for the non-segmented PCB can be verified by mounting a test cell with 17 bar clamping pressure and defined current inflow beneath the central segment via an electrical contact sheet. Results from modelling and measurement are depicted in Fig. 6 for the strongly inhomogeneous current density distribution, showing a good accordance between simulation and experiment. Currents across the corner segments 11, 13, 31 and 33 are slightly overestimated by the simulation and consequently the current across the central segment is calculated 3.4% lower than experimentally observed. However, considering measurement tolerances, material inhomogeneities and a scatter of material parameters, the simulation is yielding correct results and the methodological approach developed in this study is applicable.

As with the segmented BPP, a homogeneous current density distribution was modelled for the combination of the

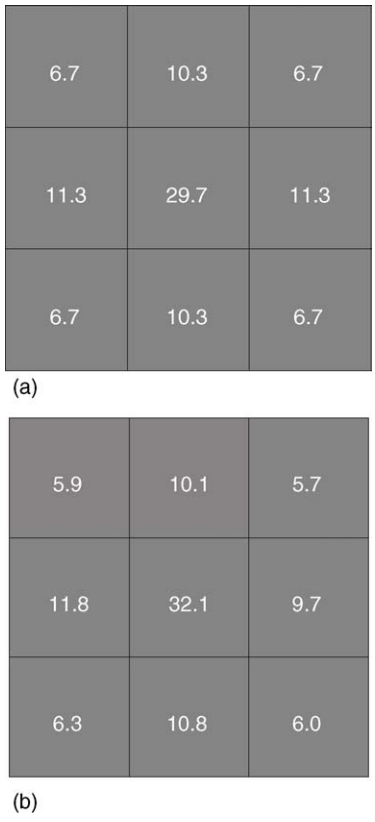

Fig. 6. (a) Simulation and (b) measurement of relative segment currents in % for strongly inhomogeneous current density distribution (non-segmented bipolar plate and printed circuit board, 3 × 3 current sensors, R_M = 7 mΩ).

non-segmented BPP and PCB. The results from the previous chapter can be assigned without any constraints, i.e. no lateral currents can be observed. Furthermore, sensitivity analysis revealed that the current density gradient between neighbouring segments and the measurement resistance R_M represent the major parameters for the occurrence of current spreading. For practical measurement configurations with an R_M of several mΩ, variations of GDL thickness, GDL through-plane resistance or contact resistances in a simulated ±20% range have a minor influence because of the strong impact of R_M [22]. This behaviour could also be confirmed experimentally by varying the clamping pressure of the test cell.

6. Comparison of measurement techniques and expansion of modelling approach

In Fig. 7, maximum lateral currents for the two approaches, i.e. relative currents across segments 21 and 23, are depicted against R_M for the strongly inhomogeneous current density distribution. Due to the non-segmented GDL, current spreading between neighbouring segments can be observed for both measurement techniques. The curve for the non-segmented BPP shows a relatively steep increase for small resistance values, followed by an almost constant characteristic. A significant gain in measurement accuracy

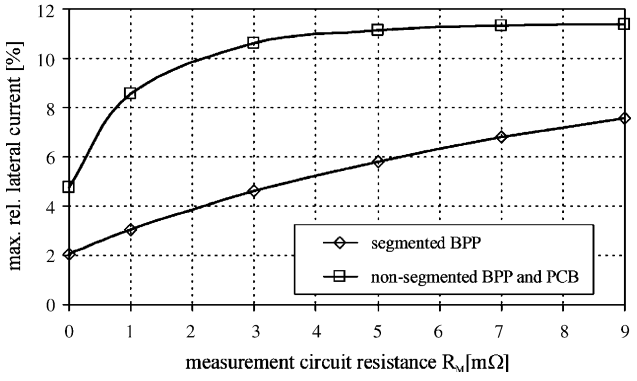

Fig. 7. Comparison of maximum lateral currents between neighbouring segments for the worst-case current density distribution scenario (BPP, bipolar plate and PCB, printed circuit board).

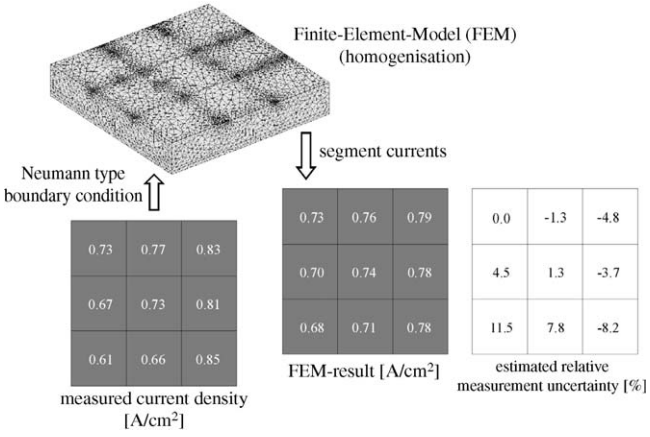

Fig. 8. Approach for estimating measurement uncertainties due to current spreading in non-segmented gas diffusion layer and non-segmented bipolar plate for a measured current density distribution (non-segmented bipolar plate and printed circuit board, 3 × 3 current sensors).

is only possible if resistance values smaller than 3 mΩ can be realized for the given configuration. The curve for the segmented BPP in contrast is monotonically increasing within the considered range of R_M and clearly demonstrates the inherently higher accuracy of this approach.

As the measurement accuracy strongly depends on the current density gradient between neighbouring segments and current distribution mapping only yields average values for individual segments, the actual uncertainty of measurement cannot be quantified accurately. Moreover, the modelling approach developed in this study cannot easily be inverted, i.e. it is not possible to evaluate the current density distribution at the electrode in a one step procedure by applying the measured current density distribution as Neumann type boundary condition at the current collector surfaces. For the electrode, neither Neumann nor Dirichlet type boundary conditions can be defined in this case and thus the system would be under-determined. However, it is possible to estimate uncertainties for a detected current density distribution by applying measured current density values as boundary conditions at the electrode surface and calculating the segment currents in the same manner as described above and exemplarily outlined in Fig. 8 [23].

Current spreading in the non-segmented GDL, and as the case may be in the non-segmented BPP, results in a homogenisation of the current density profile that can be quantified by a measurement uncertainty $u_n = (j_{\mathrm{mod},n} - j_{\mathrm{meas},n}) / j_{\mathrm{meas},n} \times 100\%$, where $j_{\mathrm{mod,n}}$ represents the simulated average current density of segment n at the current collector and $j_{\mathrm{meas,n}}$ represents the corresponding average current density that was measured and defined as boundary condition. In the example according to Fig. 8, an experimental result obtained from measurements with the PCB setup is analysed. The test cell was operated in galvanostatic mode with H_2 and air at a total cell current of 72.1 A. The MEA was GORE 5620 with 100 cm^2 active area, the other PEFC components and materials were the same as described in the Section 2 in this study. Maximum relative cross-flow can be observed towards the bottom left segment with the lowest current density, originating from the surrounding segments. Local currents at the right part of the active area are generally measured lower than they occur in reality because of a current density gradient towards the central part of the active area. Regarding the numerical values for the measurement uncertainties in Fig. 8, it must be clearly stated that these can only give estimates because the measured current density distribution serving as model input already represents a homogenised version of the true current density distribution. Thus, real measurement uncertainties will be higher than those specified in Fig. 8. However, it can be concluded that the measurement error in practical cases is significantly lower than the maximum error defined by the worst-case current density distribution scenario according to Fig. 7. Due to the fact that increasing the uniformity of the current density profile obviously coincides with improving the quality of measurement, the application of a non-segmented BPP in combination with a PCB can be regarded as a viable diagnostic tool.

7. Conclusions

The results obtained from modelling work in this study clearly demonstrate the impact of lateral currents on the accuracy of measurement for different current distribution mapping techniques. Especially, if a segmentation of the BPP is omitted, significant current spreading can be observed even for thin BPPs. With the aid of the finite element method, a detailed three-dimensional analysis of lateral currents is possible, based on numerical volume averaging of complex flowfield structures and on thin layer approximation of contact resistances. It could be demonstrated experimentally that the modelling approach yields correct results for the given geometries and material parameters. Assuming a strongly inhomogeneous current density distribution with current generation only beneath a single segment, a maximum measurement uncertainty can be defined and the impact of measurement circuit resistances can be analysed. For the

techniques chosen in this study, it can be concluded that the accuracy of measurement is increasing with decreasing R_M and with increasing homogeneity of the current density distribution generated at the triple phase boundary.

In practice, a compromise must be found between high accuracy and technical feasibility of a measurement technique. Segmenting thin BPPs is principally possible, however, it is a challenging and tedious task to guarantee for good mechanical stability and compatibility to an existing fuel cell layout, especially if higher spatial resolutions than 3×3 segments shall be realized. With regard to stack integration and flexibility, the approach with non-segmented BPP and PCB features strong benefits compared to a segmented BPP. Although the measurement uncertainty associated with non-segmented BPPs is significantly higher, it could be demonstrated by finite element estimation that the occurrence of lateral currents is less pronounced for practical current density distributions than for the strongly inhomogeneous worst-case scenario. Achieving a uniform current density profile under a variety of operating conditions is a major goal in developing and constructing PEFCs and coincides with a gain in accuracy of the measurement technique. Thus, the combination of a non-segmented BPP and PCB in fact represents a viable and flexible alternative to existing approaches for current distribution mapping in technically relevant PEFCs and in particular in fuel cell stacks. Irrespective of the chosen measurement technique, an estimation of current spreading is possible by means of finite element modelling and allows for a correct interpretation of measured current density distributions.

Acknowledgement

The authors wish to thank Dr. N. Berg, Dr. P. Kauranen and M. Mändle from SGL Technologies (Meitingen/Germany) for generously making available physical properties of graphite materials.

References

[1] A. Hakenjos, H. Muenter, U. Wittstadt, C. Hebling, J. Power Sources 131 (2004) 213–216.
[2] M. Noponen, T. Mennola, M. Mikkola, T. Hottinen, P. Lund, J. Power Sources 106 (2002) 304–312.
[3] Y.-G. Yoon, W.-Y. Lee, T.-H. Yang, G.-G. Park, C.-S. Kim, J. Power Sources 118 (2003) 193–199.
[4] G. Bender, M.S. Wilson, T.A. Zawodzinski, J. Power Sources 123 (2003) 163–171.
[5] A.B. Geiger, R. Eckl, A. Wokaun, G.G. Scherer, J. Electrochem. Soc. 151 (2004) A394–A398.
[6] M.M. Mench, C.Y. Wang, J. Electrochem. Soc. 150 (2003) A79–A85.
[7] N. Rajalakshmi, M. Raja, K.S. Dhathathreyan, J. Power Sources 112 (2002) 331–336.
[8] C. Wieser, A. Helmbold, E. Gülzow, J. Appl. Electrochem. 30 (2000) 803–807.
[9] A. Geiger, Dissertation No. 14872, Swiss Federal Institute of Technology Zurich, Zurich/Switzerland, 2002.
[10] M. Santis, R.P.C. Neto, F.N. Büchi, Proceedings of 2nd European PEFC Forum, Lucerne/Switzerland, 2003, pp. 391–397.
[11] J. Stumper, S.A. Campbell, D.P. Wilkinson, M.C. Johnson, M. Davis, Electrochim. Acta 43 (1998) 3773–3783.
[12] S.J.C. Cleghorn, C.R. Derouin, M.S. Wilson, S. Gottesfeld, J. Appl. Electrochem. 28 (1998) 663–672.
[13] D.J.L. Brett, S. Atkins, N.P. Brandon, V. Vesovic, N. Vasileiadis, A.R. Kucernak, Electrochem. Commun. 3 (2001) 628–632.
[14] S. Schönbauer, T. Kaz, H. Sander, E. Gülzow, Proceedings of 2nd European PEFC Forum, Lucerne/Switzerland, 2003, pp. 231–237.
[15] R. Kraume, German Patent No. DE 10,213,479 A 1 (2003) (in German).
[16] xcellvision GmbH (now TomoScience GbR) product information, Magnetotomography with fuel cells, Wolfsburg/Germany, 2003 (in German).
[17] D. Natarajan, T. Van Nguyen, J. Power Sources 135 (2004) 95–109.
[18] M. Noponen, T. Hottinen, T. Mennola, M. Mikkola, P. Lund, J. Appl. Electrochem. 32 (2002) 081–089.
[19] FEMLAB® support knowledge base, solution no. 902—thin film approximation, http://www.euro.comsol.com/support/knowledgebase/902.php?highlight=902, 2003.
[20] M. Roos, E. Batawi, U. Harnisch, Th. Hocker, J. Power Sources 118 (2003) 86–95.
[21] M. Mathias, J. Roth, J. Fleming, W. Lehnert, in: W. Vielstich, H. Gasteiger, A. Lamm (Eds.), Handbook of Fuel Cells—Fundamentals, Technology and Applications, John Wiley & Sons, 2003 (Chapter 46).
[22] R. Grinzinger, Diploma Thesis. Institute for Energy Economy and Application Technology, Munich University of Technology, 2003 (in German).
[23] W. Lehnert, W. Zhang, R. Eckl, Fuel Cell Research Symposium—Modelling and Experimental Verification, Zurich/Switzerland, 2004.